

# International Journal of Physical Sciences

Volume 11 Number 21 16 November , 2016

ISSN 1992-1950



*Academic  
Journals*

## ABOUT IJPS

The **International Journal of Physical Sciences (IJPS)** is published weekly (one volume per year) by Academic Journals.

**International Journal of Physical Sciences (IJPS)** is an open access journal that publishes high-quality solicited and unsolicited articles, in English, in all Physics and chemistry including artificial intelligence, neural processing, nuclear and particle physics, geophysics, physics in medicine and biology, plasma physics, semiconductor science and technology, wireless and optical communications, materials science, energy and fuels, environmental science and technology, combinatorial chemistry, natural products, molecular therapeutics, geochemistry, cement and concrete research, metallurgy, crystallography and computer-aided materials design. All articles published in IJPS are peer-reviewed.

### Contact Us

**Editorial Office:** [ijps@academicjournals.org](mailto:ijps@academicjournals.org)

**Help Desk:** [helpdesk@academicjournals.org](mailto:helpdesk@academicjournals.org)

**Website:** <http://www.academicjournals.org/journal/IJPS>

**Submit manuscript online** <http://ms.academicjournals.me/>

## Editors

### **Prof. Sanjay Misra**

*Department of Computer Engineering, School of Information and Communication Technology  
Federal University of Technology, Minna,  
Nigeria.*

### **Prof. Songjun Li**

*School of Materials Science and Engineering,  
Jiangsu University,  
Zhenjiang,  
China*

### **Dr. G. Suresh Kumar**

*Senior Scientist and Head Biophysical Chemistry  
Division Indian Institute of Chemical Biology  
(IICB)(CSIR, Govt. of India),  
Kolkata 700 032,  
INDIA.*

### **Dr. 'Remi Adewumi Oluoyinka**

*Senior Lecturer,  
School of Computer Science  
Westville Campus  
University of KwaZulu-Natal  
Private Bag X54001  
Durban 4000  
South Africa.*

### **Prof. Hyo Choi**

*Graduate School  
Gangneung-Wonju National University  
Gangneung,  
Gangwondo 210-702, Korea*

### **Prof. Kui Yu Zhang**

*Laboratoire de Microscopies et d'Etude de  
Nanostructures (LMEN)  
Département de Physique, Université de Reims,  
B.P. 1039. 51687,  
Reims cedex,  
France.*

### **Prof. R. Vittal**

*Research Professor,  
Department of Chemistry and Molecular  
Engineering  
Korea University, Seoul 136-701,  
Korea.*

### **Prof Mohamed Bououdina**

*Director of the Nanotechnology Centre  
University of Bahrain  
PO Box 32038,  
Kingdom of Bahrain*

### **Prof. Geoffrey Mitchell**

*School of Mathematics,  
Meteorology and Physics  
Centre for Advanced Microscopy  
University of Reading Whiteknights,  
Reading RG6 6AF  
United Kingdom.*

### **Prof. Xiao-Li Yang**

*School of Civil Engineering,  
Central South University,  
Hunan 410075,  
China*

### **Dr. Sushil Kumar**

*Geophysics Group,  
Wadia Institute of Himalayan Geology,  
P.B. No. 74 Dehra Dun - 248001(UC)  
India.*

### **Prof. Suleyman KORKUT**

*Duzce University  
Faculty of Forestry  
Department of Forest Industrial Engineering  
Beciyorukler Campus 81620  
Duzce-Turkey*

### **Prof. Nazmul Islam**

*Department of Basic Sciences &  
Humanities/Chemistry,  
Techno Global-Balurghat, Mangalpur, Near District  
Jail P.O: Beltalpark, P.S: Balurghat, Dist.: South  
Dinajpur,  
Pin: 733103,India.*

### **Prof. Dr. Ismail Musirin**

*Centre for Electrical Power Engineering Studies  
(CEPES), Faculty of Electrical Engineering, Universiti  
Teknologi Mara,  
40450 Shah Alam,  
Selangor, Malaysia*

### **Prof. Mohamed A. Amr**

*Nuclear Physic Department, Atomic Energy Authority  
Cairo 13759,  
Egypt.*

### **Dr. Armin Shams**

*Artificial Intelligence Group,  
Computer Science Department,  
The University of Manchester.*

## Editorial Board

**Prof. Salah M. El-Sayed**

*Mathematics. Department of Scientific Computing,  
Faculty of Computers and Informatics,  
Benha University. Benha ,  
Egypt.*

**Dr. Rowdra Ghatak**

*Associate Professor  
Electronics and Communication Engineering Dept.,  
National Institute of Technology Durgapur  
Durgapur West Bengal*

**Prof. Fong-Gong Wu**

*College of Planning and Design, National Cheng Kung  
University  
Taiwan*

**Dr. Abha Mishra.**

*Senior Research Specialist & Affiliated Faculty.  
Thailand*

**Dr. Madad Khan**

*Head  
Department of Mathematics  
COMSATS University of Science and Technology  
Abbottabad, Pakistan*

**Prof. Yuan-Shyi Peter Chiu**

*Department of Industrial Engineering & Management  
Chaoyang University of Technology  
Taichung, Taiwan*

**Dr. M. R. Pahlavani,**

*Head, Department of Nuclear physics,  
Mazandaran University,  
Babolsar-Iran*

**Dr. Subir Das,**

*Department of Applied Mathematics,  
Institute of Technology, Banaras Hindu University,  
Varanasi*

**Dr. Anna Oleksy**

*Department of Chemistry  
University of Gothenburg  
Gothenburg,  
Sweden*

**Prof. Gin-Rong Liu,**

*Center for Space and Remote Sensing Research  
National Central University, Chung-Li,  
Taiwan 32001*

**Prof. Mohammed H. T. Qari**

*Department of Structural geology and remote sensing  
Faculty of Earth Sciences  
King Abdulaziz UniversityJeddah,  
Saudi Arabia*

**Dr. Jyhwen Wang,**

*Department of Engineering Technology and Industrial  
Distribution  
Department of Mechanical Engineering  
Texas A&M University  
College Station,*

**Prof. N. V. Sastry**

*Department of Chemistry  
Sardar Patel University  
Vallabh Vidyanagar  
Gujarat, India*

**Dr. Edilson Fereda**

*Graduate Program on Knowledge Management and IT,  
Catholic University of Brasilia,  
Brazil*

**Dr. F. H. Chang**

*Department of Leisure, Recreation and Tourism  
Management,  
Tzu Hui Institute of Technology, Pingtung 926,  
Taiwan (R.O.C.)*

**Prof. Annapurna P.Patil,**

*Department of Computer Science and Engineering,  
M.S. Ramaiah Institute of Technology, Bangalore-54,  
India.*

**Dr. Ricardo Martinho**

*Department of Informatics Engineering, School of  
Technology and Management, Polytechnic Institute of  
Leiria, Rua General Norton de Matos, Apartado 4133, 2411-  
901 Leiria,  
Portugal.*

**Dr Driss Miloud**

*University of mascara / Algeria  
Laboratory of Sciences and Technology of Water  
Faculty of Sciences and the Technology  
Department of Science and Technology  
Algeria*

**Prof. Bidyut Saha,**

*Chemistry Department, Burdwan University, WB,  
India*

**ARTICLES**

**Investigation of self-association, optical transition probability and hetero-association with chlorogenic acid of nicotinamide using UV-Vis spectroscopy** 269

Ataklti Abraha, Ashok Gholap and Abebe Belay

**Baryte mineral exploration in parts of the lower Benue Trough, Nigeria** 279

C. N. Ehirim, J. O. Ebeniro and C. O. Ofoegbu

*Full Length Research Paper*

# Investigation of self-association, optical transition probability and hetero-association with chlorogenic acid of nicotinamide using UV-Vis spectroscopy

Ataklti Abraha<sup>1,2\*</sup>, Ashok Gholap<sup>2</sup> and Abebe Belay<sup>3</sup>

<sup>1</sup>Department of Physics, School of Natural and computational Sciences, Samara University, P. O. Box 132, Samara, Ethiopia.

<sup>2</sup>Department of physics, College of Natural Science, Addis Ababa University, P. O. Box 1176, Addis Ababa, Ethiopia.

<sup>3</sup>Department of Physics, School of Natural Sciences, Adama Science and Technology University, P. O. Box 1888, Adama, Ethiopia.

Received 15 August, 2016; Accepted 24 October, 2016

The self-association, optical transition probabilities, and hetero-association with chlorogenic acid of nicotinamide were obtained from UV-Vis spectroscopy in aqueous solution at room temperature (293K). The dimerization constant of nicotinamide ( $2.378 \times 10^4 M^{-1}$ ) was obtained using dimer model by nonlinear curve fitting technique. The hetero-association constant ( $4.31 \times 10^3 M^{-1}$ ) in the system of molecules of nicotinamide with chlorogenic acid were obtained in aqueous solution using a Benesi-Hildebrand equation. In order to characterize the binding system of the dimerization reactions for the self and hetero-association of the compound, the thermodynamic parameters were investigated using Vant's Hoff equation at the temperature range (293 to 299K). As a result, the change of enthalpy obtained for the self and hetero-association is  $(4.826 \pm 0.415) kJ.mol^{-1}.K^{-1}$  and  $-(16.928 \pm 0.836) kJ.mol^{-1}.K^{-1}$  respectively. The values of change in the thermodynamic parameters indicated that the hydrophobic interaction and electrostatic forces subsequently plays the major role in the binding reaction between the molecules of nicotinamide and its complexes with chlorogenic acid, respectively. In addition, the optical transition probabilities of nicotinamide were also calculated in the wavenumber regions ( $36127.17 - 40453.07 cm^{-1}$ ) by using integrated absorption coefficient techniques. Finally, the results of this study are very important for understanding the binding reaction in biological system, nature and strength of the transition in molecular interaction, absorption spectral interpretation, and in providing stringent test of atomic and molecular structure calculations in theoretical work of the compounds.

**Key words:** Nicotinamide, chlorogenic acid, self-association, hetero-association, optical transition probabilities, thermodynamic properties, UV-Vis spectroscopy.

## INTRODUCTION

Vitamins are organic chemical compounds, which are very important for an organism as a vital nutrient to sustain life

since they play an important role in normal metabolism process, growth and vitality (Hassan, 2012). Nicotinamide

(Vitamin B3) is an active, water soluble and amide form vitamin that is found in small amounts in natural foodstuff (Hassan, 2012). It can be obtained through synthesis in the body or as a dietary source and supplement of different food sources such as chicken, pork, beef, fish, legumes, nuts, grain products, mushrooms, yeast extracts, and coffee (Hassan, 2012; FSANZ, 2011; DiPalma and Thayer, 1991). It functions to the coenzymes nicotinamide adenine dinucleotide (NADH) and nicotinamide adenine dinucleotide phosphate (NADP), and is a precursor of essential enzymatic reactions in the body including adenosine triphosphate (ATP) production (Williams and Ramsden, 2005; Rolfe, 2014; Shalita and Smith, 1995; Jackson et al., 1995). Lack of nicotinamide leads to pellagra, fatigue, loss of appetite, pigmented rashes of the skin, oral ulcerations, dermatitis, dementia and death (Maiese et al., 2009; Hegyi et al., 2004).

Functional foods and bioactive components such as chlorogenic acid of different fruits and vegetables are beneficial for human health (Liu, 2003; Crowe, 2013) and because they present in popular drinks and foods (that is, in coffee, tea, cola beverages and chocolates). They are the most widely consumed of all behaviorally active drugs in the world (Clifford, 1979; Bolton and Null, 1981). Chlorogenic acid (CGA) is a main phenolic natural product that possesses many health benefits, including antioxidative (Wen et al., 2004; Richelle et al., 2001; Ayaz et al., 2008), antibiotic, anti-hypercholesterolemia, antihypertensive (Svilaas et al., 2004), as a selective inhibitor for the production of glucose in liver (Schwab, 2001), in plant metabolism or glucose absorption (Svilaas et al., 2004), used in disorders such as obesity, diabetes, and cancer (Wang et al., 2008; Clifford et al., 2010), chemopreventive, and other biological activities (Nazzaro et al., 2009).

With the increasing use of food supplements and the rapid development of new types of drugs, food/drug interactions are currently a great field of interest. Interaction of bioactive compounds with vitamins and aromatic drugs is one of the most common study areas, since the compounds can be found in various food sources and the interaction may affect the pharmacodynamics and pharmacokinetics of the compounds (Crowe, 2013). Thus, this study is important because knowledge of the association, optical transitional probability and thermodynamic parameters are very important for understanding the binding reaction in biological system, nature and strength of the molecular interaction in liquid solutions, to characterize the electron transition probabilities, interpreting the absorption spectra, and in providing stringent test of atomic and

molecular structure calculation in theoretical works (Belay, 2013; Bayliss, 1950; Mac Rae, 1957; Milonni and Eberly, 1988; Ataklti et al., 2016). Chlorogenic acid was studied for self and hetero-association with ethidium bromide (EB) (Belay, 2013) and with five antibiotics drugs (amikacin, ampicillin, ciprofloxacin, erythromycin, and vancomycin) for the application against bacteria (Hemaiswarya and Doble, 2010). To the best of our knowledge the self and hetero-association, optical transitional probability and thermodynamic parameters of the nicotinamide to elucidate structures, optical transition and thermodynamic properties of the molecules are not yet investigated using UV-Vis spectroscopy. UV-Vis spectroscopy is the simplest techniques to study such kind of interactions, since the technique is highly sensitive, rapid and can be easily implemented (Belay, 2013; Niazi et al., 2006; Ataklti et al., 2016). Therefore, the objective of this work is to investigate the self-association, optical transition probability and hetero-association with chlorogenic acid of nicotinamide using UV-Vis spectroscopy.

## MATERIALS AND METHODS

Nicotinamide (NIC, Figure 1a) and chlorogenic acid (CGA, Figure 1b) from Sigma-Aldrich were used for measurements without any further purification. All solutions were made using doubly distilled water. The solutions were stored in the dark to avoid photo degradation of the compounds. For the electronic absorption measurements of the solutions, Perkin-Elmer Lambda 19 UV-Vis Spectrophotometry with double monochromator using 1 cm fused quartz cuvette in a spectrum range 200 to 500 nm was used at room temperature (293K). The analyzed spectra were obtained by subtracting the spectrum of pure solvent (water) from that of the solution containing of the compounds. A digital balance with accuracy of 0.0001 g, measuring cylinders, pipettes, and volumetric flasks, magnetic stirrer with hot plate and beakers where also used.

The self-association of NIC was studied over the concentration range of  $(2.234 - 1.055) \times 10^{-4} M$ . The absorbance as a function of concentration has been measured at absorption maxima 261.6 nm to obtain the greatest accuracy of detection. For numerical analysis of the self-association, dimer model equation was used by fitting to the experimental data using non-linear curve fitting based on Levenberg-Marquardt algorithm using Origin 8 software (Ataklti et al., 2016; Belay, 2010). The molar extinction coefficients and equilibrium constants were used as searching parameters, in order to achieve minimum discrepancy between the experimental data and equations.

Moreover, the complexation of NIC-CGA the constant NIC concentration  $8.49 \times 10^{-5} M$  was titrated by CGA solutions in a concentration range of  $(1.221 - 1.196) \times 10^{-4} M$ . The numerical values of the association constant and molar extinction coefficient of the complexes between NIC-CGA at their maximum wavelength was analyzed using the Benesi-Hildebrand approach by

\*Corresponding author. E-mail: atklt.physics@gmail.com.

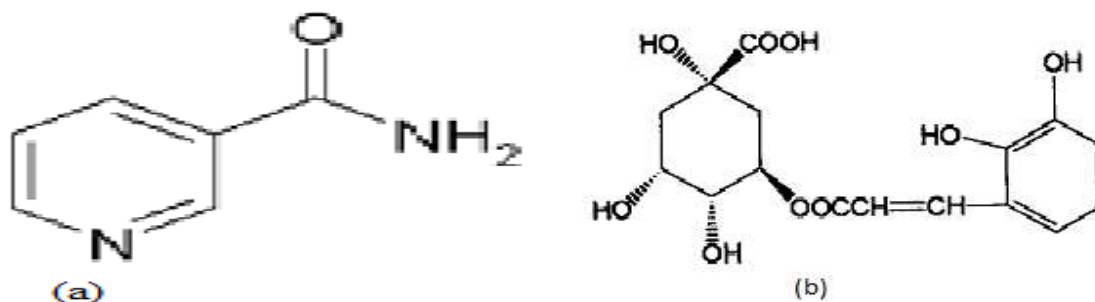


**Figure 1.** Chemical structure of (a) nicotinamide and (b) chlorogenic acid.

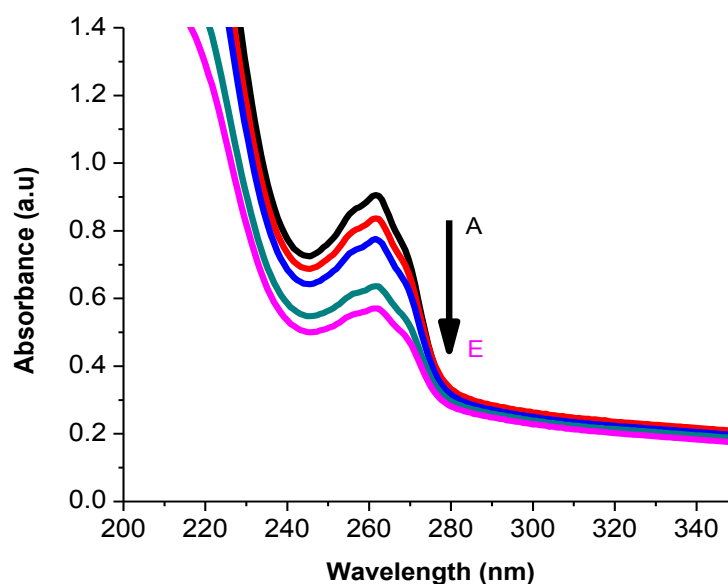


**Figure 2.** Absorbance of nicotinamide A – E of concentration  $(2.234-1.055)\times 10^{-4} M$

a linear curve fitting for the experimental data with that of the theoretical values obtained from equation (16) using Origin 8 software.

Similarly, the thermodynamic parameters such as enthalpy, gibbs free energy and entropy of the self-association of NIC and its hetero-association with CGA were studied at the temperature range (293 to 299K), respectively. These parameters have been determined using the model of Vant's Hoff's equation by linear curve fitting for the experimental data with that of the theoretical values.

The integrated absorption technique which is more powerful in measuring the intensity of absorption light has been used to calculate the optical transition probabilities (transition dipole moment, oscillator strength and integrated absorption cross-section) (Ataklti et al., 2016; Belay, 2010; Belay, 2013). The pure nicotinamide was studied by integrating the absorption coefficient and molar decadic absorption coefficients in the wave number regions of 20000 to 40000  $\text{cm}^{-1}$ . Usually, the UV-Vis spectrophotometer measures the concentration in terms of absorbance versus wavelength; this was recalculated into absorption coefficient or molar decadic absorption coefficient versus wave number using Origin 8 software.

## RESULTS AND DISCUSSION

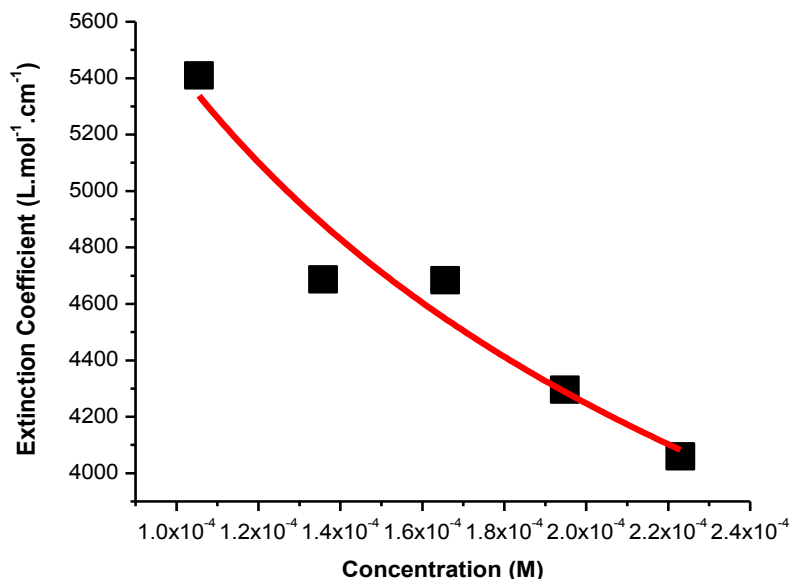
### Self-association of nicotinamide

Figure 2 shows the concentration dependence of self-association spectra of NIC measured in dually distilled water at room temperature (293K) with one absorption peak observed at the wavelength 261.6 nm. The quantitative analysis for self-association of nicotinamide was carried out using the concentration dependent molar extinction coefficient of the molecules at its maximum wavelength.

Numerical analysis was carried out using dimer model and the equation derived according to the following molecular equilibrium in solutions (Belay, 2010; Belay, 2012; Ataklti et al., 2016).







**Figure 3.** Molar extinction coefficient versus concentration of NIC under the peak of 261.6 nm.

where  $C_1$  and  $C_2$  are monomers and dimers of the compound, respectively and  $K_E$  is the equilibrium dimerization constant. The overall concentration of the dissolved molecules in the solution, using the mass conservation law can be written as:

$$[C_0] = [C_1] + 2[C_2] \quad (2)$$

where  $[C_0]$  is the total concentration and

$$[C_2] = K_E [C_1]^2.$$

The contribution of the monomer and dimer to the molar extinction coefficient of the solution is commonly considered to be additive and

$$\varepsilon = \varepsilon_m f_m + \varepsilon_d f_d \quad (3)$$

$$f_m = \frac{[C_1]}{[C_0]} \quad (4)$$

$$f_d = 2K_E \frac{[C_1]^2}{[C_0]} \quad (5)$$

where  $\varepsilon_m$ ,  $\varepsilon_d$ ,  $f_m$  and  $f_d$  are molar monomer extinction coefficients, molar dimer extinction coefficients, equilibrium mole fraction of the molecules in the

monomer concentration and equilibrium mole fraction of the molecules in the dimer concentration, respectively.

The concentration can be derived from the mass conservation law given in equation (2) by substituting on the account of equation (3). Thus, the known dimer model is obtained as,

$$\varepsilon = \varepsilon_d + (\varepsilon_d - \varepsilon_m) \frac{1 - \sqrt{8[C_0]K_E + 1}}{4[C_0]K_E}. \quad (6)$$

In Equation 6, there are three unknown parameters  $\varepsilon_m$ ,  $\varepsilon_d$  and  $K_E$  which can be obtained from fitting dimer model equation to the experimental data as shown in Figure 3. The obtained values of the dimerization constants  $K_E$ , monomer extinction coefficient and dimer extinction coefficient of NIC at wavelength 261.6 nm are  $2.378 \times 10^4 M^{-1}$ ,  $1.389 \times 10^4 M^{-1}.cm^{-1}$  and  $5.74 \times 10^2 M^{-1}.cm^{-1}$ , respectively. The deviation of the Beer-Lambert's law at high concentration and dependence on concentration, suggest the existence of self-association process of the molecule (Antonov et al., 1999; Belay, 2012). The existence of self-association of nicotinamide may modify the pharmacokinetic properties of the compound.

Figure 4 shows the mole fraction of monomer and dimer versus concentration of nicotinamide molecules under the peak of 261.6 nm. The graphs show increase and decrease in the mole fraction of dimer and monomer as the concentrations of the NIC is increasing and it

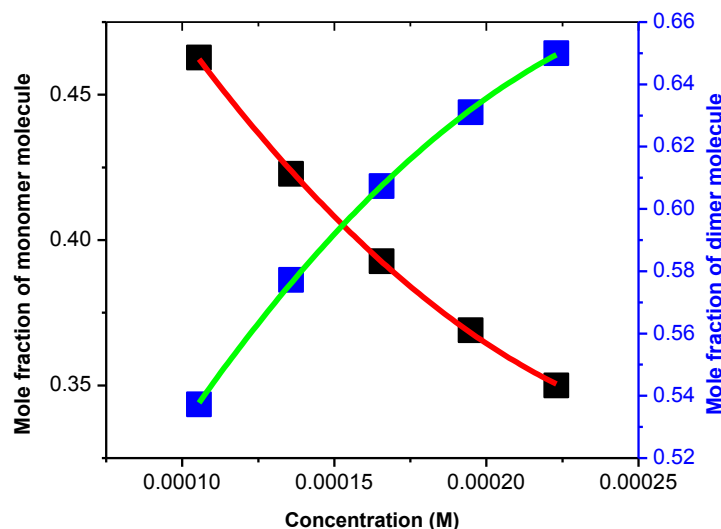


**Figure 4.** The mole fraction of monomer and dimer versus total concentration of NIC under the peak of 261.6 nm.

indicates the presence of dimerization at low concentration of NIC and more favored at high concentration of the compound.

#### Hetero-association of nicotinamide with chlorogenic acid

The mathematical approach used in physical chemistry for the determination of equilibrium constant called Benesi-Hildebrand approach were used for the quantitative analysis interaction of nicotinamide with chlorogenic acid (Benesi, 1949), under the condition  $[C_0] \gg [D_0]$ . A constant of nicotinamide solution ( $C_{NIC} = [D_0] = 8.49 \times 10^{-5} M$ ) with different concentrations range ( $C_{CGA} = [C_0] = (1.24 - 1.196) \times 10^{-4} M$ ) of chlorogenic acid solutions were used to calculate the equilibrium constant and molar extinction coefficient of the interaction formation. When a chromophoric precursor is converted to product with different spectrums an isosbestic point is observed in overlaid spectra. In more complex reactions, the wavelength of isosbestic also changes if the molar absorptivity of the precursor changes and the fraction of the precursor converted to multiple product changes (Antonov et al., 1999). Figure 5 shows the effects of CGA concentration on the UV-Vis absorption spectra of NIC solutions. The addition of CGA to NIC solutions results in important spectral modification and red band shift were observed. As shown in Figure 5, the absorbance of NIC increases when CGA is added to the NIC solution. This indicates that, CGA promotes NIC for its pharmaceutical function. Moreover, the existences of isosbestic points were observed at wavelength of about 258 and 265 nm of the interaction which indicates

the formation of complexes between CGA with NIC (Khopkar, 1998).

The equilibrium constant for the complex formation  $K_E$ , is derived as:



From Equation 7, the equilibrium constant for the complex formation  $K_E$  can be defined as:

$$K_E = \frac{[CD]}{[C][D]}, \quad (8)$$

where  $[C]$ ,  $[D]$ , and  $[CD]$  are the equilibrium concentration of CGA, NIC, and association of NIC-CGA, respectively. The initial concentration of NIC and CGA is designated as:

$$[D_0] = [D] + [CD], \quad (9)$$

$$[C_0] = [C] + [CD]. \quad (10)$$

Substituting Equations 9 and 10 into Equation 8 gives,

$$K_E = \frac{[CD]}{([D_0] - [CD])([C_0] - [CD])}. \quad (11)$$

For  $[C] \gg [D]$ , then  $[C_0] - [CD] \approx [C_0]$ . So, Equation 11 can be written as,

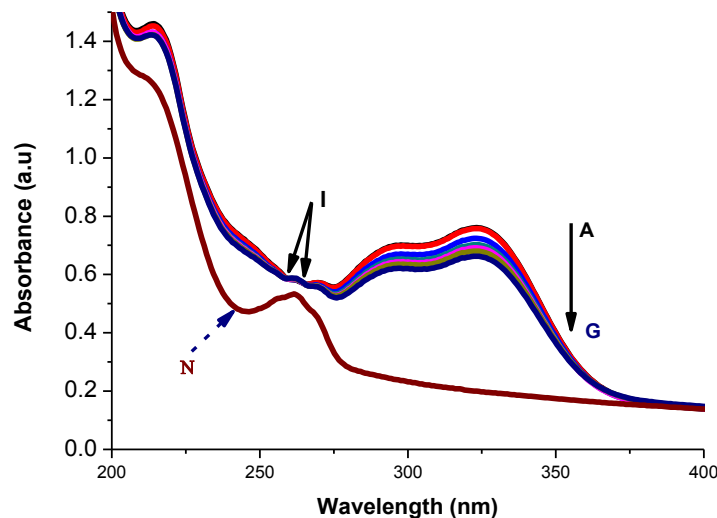


**Figure 5.** The absorbance versus different concentration of chlorogenic acid A to G ( $C_{CGA} = [C_0] = (1.24 - 1.196) \times 10^{-4} M$ ) and NIC ( $C_{NIC} = [D_0] = 8.49 \times 10^{-5} M$ ) = constant, N is the spectra of Nic alone.

$$K_E = \frac{[CD]}{([D_0] - [CD])[C_0]} \quad (12)$$

After re-arranging Equation 12, we have

$$[CD] = \frac{K_E [D_0] [C_0]}{(1 + K_E [C_0])}. \quad (13)$$

The absorbance (A) for concentration [CD] according to Beers law is

$$A = [CD] \varepsilon l = \varepsilon l \frac{K_E [D_0] [C_0]}{(1 + K_E [C_0])} \quad (14)$$

By re-arranging Equation 14, we obtain

$$\frac{[D_0]}{A} = \frac{1 + K_E [C_0]}{\varepsilon l K_E [C_0]} \quad (15)$$

When the path length  $l$  of the cuvette is 1 cm, Equation 15 can be written in the form of Benesi-Hildebrand equation as:

$$\frac{[D_0]}{A} = \frac{1}{\varepsilon} + \frac{1}{\varepsilon K_E [C_0]}. \quad (16)$$

The plot of  $\frac{D_0}{A}$  vs  $\frac{1}{[C_0]}$  gives a straight line with y-intercept  $\frac{1}{\varepsilon}$  and slope  $\frac{1}{\varepsilon K_E}$  as shown in Figure 6. Thus,

the equilibrium constant and molar extinction coefficient calculated by fitting Equation 16 to experimental data of Figure 6 are  $4.3135 \times 10^3 M^{-1}$  and  $4.903 \times 10^3 M^{-1} \cdot cm^{-1}$  respectively. The obtained results are in a good agreement with the results  $1.18 \times 10^3 M^{-1}$  (Abraha et al., 2016) for the equilibrium constant for the complex formation.

#### Thermodynamic properties of self and hetero-association with CGA of nicotinamide

Heating the aqueous solution of NIC, NIC-CGA complex shows that the absorption spectra of the molecules are strongly dependent on the temperature in the range of 293 to 299K. The equilibrium constants of the molecules of the compounds at the aforementioned temperature were calculated at the peak of wavelengths of the self and hetero association using Equations 3 and 16, respectively. Figure 7a and b, shows the graph of  $\ln K_E$  versus  $f(\frac{1}{T})$  of NIC and its hetero-association with CGA.

The magnitude of the enthalpy was estimated from the slope of the approximating line according to Vant's Hoff's equation:

$$\frac{d \ln(K_E)}{f(\frac{1}{T})} = -\frac{\Delta H}{R}, \quad (17)$$

where  $\Delta H$  is the molar enthalpy change,

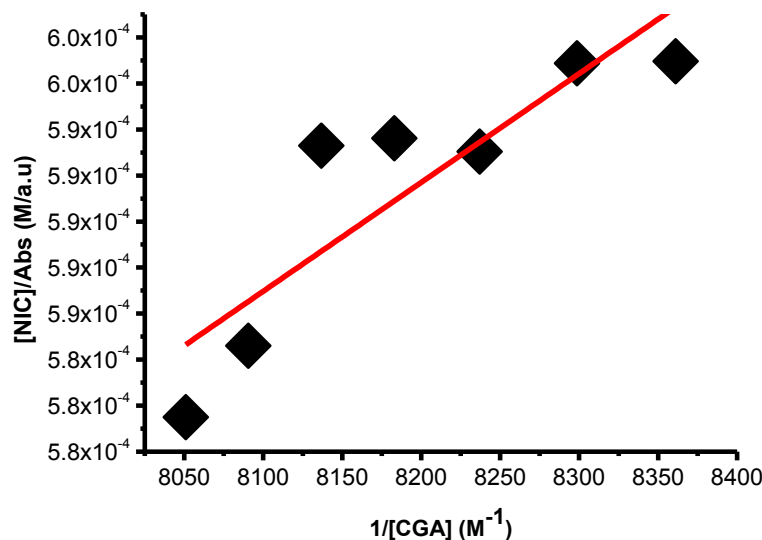


Figure 6. Concentration of NIC/Abs versus 1/concentration of CGA at  $\lambda_{max}$  213.6.

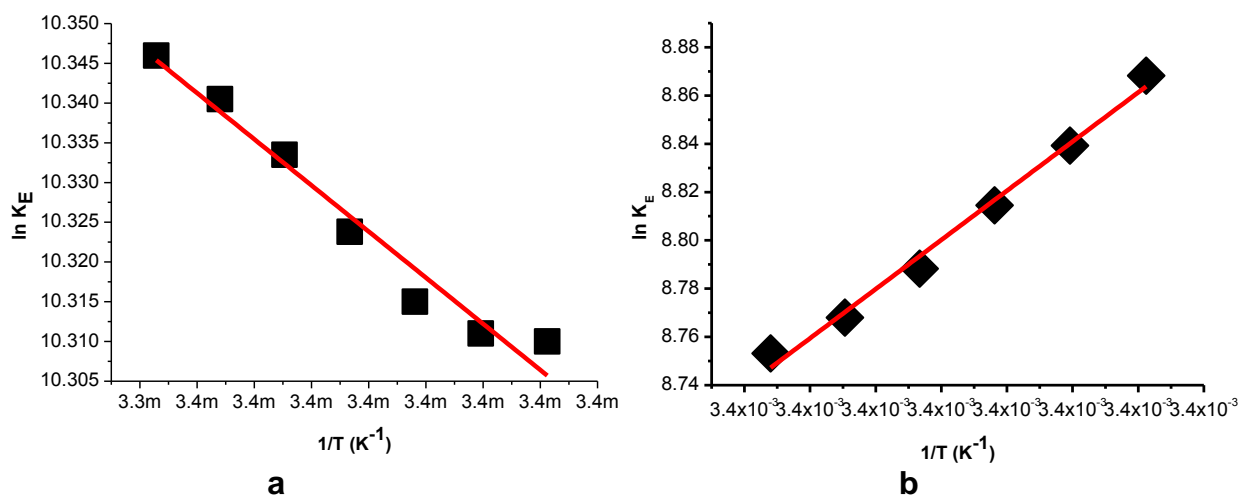


Figure 7 (a)  $\ln K_E$  versus  $1/T$  of NIC at concentration of  $(4.5 \times 10^{-4} M)$ . (b)  $\ln K_E$  versus  $1/T$  of NIC+CGA at concentration CGA  $(4.027 \times 10^{-4} M)$  and NIC  $(4.5 \times 10^{-4} M)$ .

$R = 8.31 J.mol^{-1}K^{-1}$  is the universal gas constant and  $T$  the temperature in Kelvin. The entropy was derived from Gibb's free energy and enthalpy. The change Gibb's free energy and entropy can be expressed as:

$$\Delta G = -RT \ln(K_E), \tag{18}$$

$$\Delta S = -\frac{\Delta G - \Delta H}{T}. \tag{19}$$

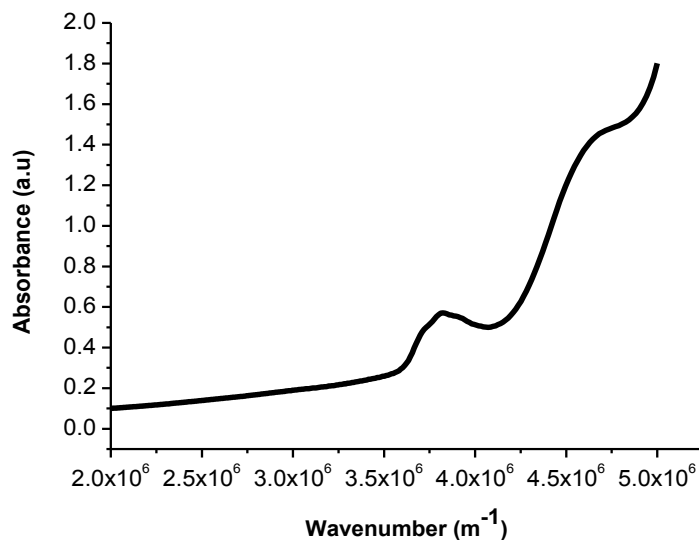
Finally, the Vant's Hoff's equation can be given by

$$\ln K_E = \frac{\Delta S}{R} - \frac{\Delta H}{R} \frac{1}{T}. \tag{20}$$

Plots of  $\ln K_E$  versus  $T^{-1}$  gives a straight line, whose slope and intercept can be used to determine  $\Delta S$  and  $\Delta H$  and Gibb's free energy can be determined at a specific temperature using Equation 19. In order to characterize the force between NIC and NIC-CGA molecules, thermodynamic parameters on the given temperatures were analyzed using Vant's Hoff's equation. The thermodynamic parameters, Gibb's free energy change

**Table 1.** Calculated result of the thermodynamic parameters of NIC and NIC-CGA at a temperature range 293 to 299K.

Parameter	Values	
	NIC	NIC-CGA
$\Delta G / kJ.mole^{-1}$	$-(25.11 \pm 0.004)$	$-(21.59 \pm 1.665)$
$\Delta H / kJ.mole^{-1}$	$4.826 \pm 0.415$	$-(16.927 \pm 0.836)$
$\Delta S / kJ.mole^{-1}.K^{-1}$	$0.102 \pm 0.0014$	$0.015 \pm 0.003$

**Figure 8.** Absorbance versus wavenumber of nicotinamide at  $1.055 \times 10^{-5} M$ 

( $\Delta G$ ), enthalpy change ( $\Delta H$ ) and entropy change ( $\Delta S$ ) are important for confirming the binding mode. The calculated values for the Gibb's free energy, enthalpy, and entropy of the molecules for the self and hetero association is obtained as Table 1. Since  $\Delta H > 0$  and  $\Delta S > 0$ , hydrophobic interactions are dominant for the interaction of NIC molecules, but for the interaction between NIC-CGA ( $\Delta H < 0$  and  $\Delta S > 0$ ), electrostatic forces plays the major role in the interaction. Moreover, the negative value for the Gibb's free energy and enthalpy indicates that the absorption process of the compounds is continuous and exothermic reaction, respectively, and the positive value of enthalpy for the self-association shows that the process is endothermic reaction. Also, the positive value of entropy confirms the increasing randomness of the solution interface during the absorption process of the molecules of the compounds (Guo et al., 2014). The calculated result for change in entropy of the complexation is also similar with the previously reported thermodynamic results given by  $\Delta S = 0.037 kJ.K^{-1}.mol^{-1}$  for Chlorogenic Acid in  $\beta$ -cyclodextrin Complex (Álvarez-Parrilla et al., 2010).

### Optical transition properties of nicotinamide

Figure 8 represents the absorbance versus wavenumber obtained from the UV-Vis absorption spectra in water solvent at a concentration of  $1.055 \times 10^{-5} M$ . The optical transition probabilities of nicotinamide were obtained from the absorption spectra to characterize the strength of the electron transition and to interpret the absorption spectra. The molar decadic absorption coefficient which represents the ability of a molecule to absorb light in a given solvent at a given wavelength were calculated using Beer-Lambert's law (Belay, 2013; Liptay, 1969) and integrated absorption coefficient is the sum of absorption coefficient for all frequencies. It is independent of line function which may be varying due to pressure, temperature, interaction of solute and solvent (Milonni and Eberly, 1988; Michale, 1999). The integrated absorption coefficient ( $\alpha_i$ ) in the frequency ( $\nu + d\nu$ ) regions can be expressed by,

$$\alpha_i = \int \alpha d\nu \quad (21)$$

**Table 2.** Calculated results of the optical transition probabilities of NIC

Parameter	Values
Concentration ( $\text{mol.L}^{-1}$ )	$1.055 \times 10^{-5} M$
$\lambda_{\text{max}} / \varepsilon_{\text{max}}$ ( $\text{nm} / \text{m}^2 \cdot \text{mol}^{-1}$ )	$261.6 / (541.14 \pm 0.089)$
$\alpha_i / \text{m}^{-2}$	$(2.175 \pm 0.235) \times 10^5$
$\sigma_i / \text{m.molecule}^{-1}$	$(3.425 \pm 0.343) \times 10^{-15}$
$f$	$0.089 \pm 0.002$
$\mu_{km} / \text{C.m}$	$(7.41 \pm 0.063) \times 10^{-30}$

The integrated absorption cross-section ( $\sigma_i$ ) is given by Milonni and Eberly (1988):

$$\sigma_i = \frac{1}{N} \int \alpha dv \quad (22)$$

where  $\alpha$  is absorption coefficient and N is number density of the molecules.

Oscillator strength which represents the average number of electrons per atom that can be excited by the incident radiation which is an important parameter for providing the relative strength of electron transition and can be related as follows with the molar decadic absorption coefficient ( $\varepsilon$ ) as a function of frequency (Georgakopoulos et al., 2004):

$$f = 4.32 \times 10^{-9} \frac{\text{mol.cm}}{L} \int \varepsilon(v) dv \quad (23)$$

The transition dipole moment ( $\mu_{km}$ ) is a vector that depends on both ground state and excited state and couple the transition to the electric field of light and it is related with molar decadic absorption coefficient as (Liptay, 1969; Michale, 1999):

$$S \frac{|\mu_{km}|^2}{3} = \int \frac{\varepsilon(v) dv}{v} \quad (24)$$

where  $S = 2.9352 \times 10^{60} \text{C}^{-2} \text{mol}^{-1}$ . Using the Equations (21, 22, 23 and 24), the optical transition properties of nicotinamide calculated in bi-distilled water are presented in Table 2. The peak in the visible region of the compounds is due to  $\pi \rightarrow \pi^*$  electronic transitions of chromophore groups (Bakhshiev, 1961; Firth et al., 1983).

## Conclusions

The result of this investigation indicates that the molecule

of nicotinamide aggregates with itself and with chlorogenic acid molecules in the solution. The calculated parameters for the self and hetero-association are important implication for interpreting the study of binding and kinetic chemical reaction system of the compounds. These parameters are very useful for understanding the nature and strength of its molecular interaction in liquid solutions, in order to characterize the electron transition probabilities and interpret the absorption spectra of the compound, for direct experimental application in the emission, absorption and dispersion and in providing stringent test of atomic and molecular structure calculation in theoretical works. In addition, knowledge of the mechanism of the association, thermodynamic properties and the optical transition probabilities of NIC are useful in order to design the advanced and controllable carriers of drugs and food components. Therefore, the investigated results have wider applications in optical characterization, pharmaceutical drug designing and food companies in terms of economic and scientific utility.

## Conflict of Interests

The authors have not declared any conflict of interests.

## ACKNOWLEDGEMENTS

The authors wish to acknowledge the generous grant by International Science Program (ISP) of Uppsala University, Uppsala, Sweden. They are grateful to Dr. Mulugeta for providing facilities at Polymer Laboratory of Physics Department, CNS, AAU.

## REFERENCES

- Abraha A, Kebede A, Belay A (2016). Study of the self-association of amoxicillin, thiamine and the hetero-association with biologically active compound chlorogenic acid. *Afr. J. Pharm. Pharmacol.* 10(18):393-402.
- Álvarez-Parrilla E, Palos R, de la Rosa LA, Frontana-Urbe, BA,

- González-Aguilar GA, Machi L, Ayala-Zavala JF (2010). Formation of Two 1:1 Chlorogenic Acid:  $\beta$ -cyclodextrin Complexes at pH 5: Spectroscopic, Thermodynamic and Voltammetric study. *J. Mex. Chem. Soc.* 54(2):103-110.
- Ataklti A, Gholap AV, Abebe B (2016). Study self-association, optical transition properties and thermodynamic properties of neomycin sulfate using UV-Visible spectroscopy. *Int. J. Biophys.* 6(2):16-20.
- Antonov L, Gergov G, Petrov V, Kubista M, Nygren J (1999). UV-vis spectroscopic and chemo metric study on aggregation of ionic dyes in water. *Talanta* 49:99-106.
- Ayaz FA, Hayirlioglu-Ayaz S, Alpaya-Karaoglu S, Gruz J, Valentova K, Ulrichova J (2008). Phenolic acid contents of kale (*Brassica oleracea* L. var. *acephala* DC.) extracts and their antioxidant and antibacterial activities. *Food Chem.* 107:19-25.
- Bakhkshiev NG (1961). Universal intermolecular interactions and their effects on the position and electronic spectra of molecules in two components solutions. *Optic. Spectrosc.* 10:379-384.
- Bayliss NS (1950). The effect of electrostatic polarization of solvent on electronic absorption spectra in solution. *J. Chem. Phys.* 18:292.
- Belay A (2010). Determination of self - associated 5- caffeoylquinic acid and its complexation with sodium hydroxide using UV-Vis spectroscopy. *Int. J. Phys. Sci.* 5(5):459-464.
- Belay A (2012). Spectrophotometric method for the determination of caffeic acid complexation and thermodynamic properties. *Int. J. Biophys.* 2:12-17.
- Belay A (2013). The hetero-association of caffeine with 5-caffeoylquinic acid and ethidium bromide. *J. Bio. Phys. Chem.* 13: 30–35.
- Benesi HA (1949). Spectrophotometric investigation of iodine with aromatic hydrocarbons. *J. Am. Chem. Soc.* 71:2703-2707.
- Bolton S, Null G (1981). Caffeine, psychological effect, use and abuse. *J. Orthomol. Psychiatry* 10:202-211.
- Clifford MN (1979). Chlorogenic acid their complex nature and routine determination in coffee beans. *J. Sci. Food Agr.* 27:73-84.
- Clifford MN, Wu W, Kirkpatrick J, Jaiswal R, Kuhnert N (2010). Profiling and characterization by liquid chromatography/multi-stage mass spectrometry of the chlorogenic acids in *Gardenia Fructus*. *Rapid Commun. Mass Spectrom.* 24:3109-3120.
- Crowe KM (2013). Designing Functional Foods with Bioactive Polyphenols: Highlighting Lessons Learned from Original Plant Matrices. *J. Hum. Nutr. Food Sci.* 1(3):1018.
- DiPalma JR, Thayer WS (1991). Use of niacin as a drug. *Annu. Rev. Nutr.* 11:169-187.
- Firth WJ, Watkins CL, Graves DE, Yielding LW (1983). Synthesis and characterization of ethidium analogs, emphasis on amino and azido substituent. *J. Heterocycl. Chem.* 20:759-765.
- Food Standards Australia New Zealand (2011). NUTTAB 2010 – Australian Food Composition Tables. Canberra: FSANZ.
- Georgakopoulos S, van Grondelle R, vander Zwan G (2004). Circular dichroism of Carotenoides in bacterial light-harvesting complexes: experimental and modeling. *Biophys. J.* 87:3010-3022.
- Guo Y, Liu B, Li Z, Zhang L, Lv Y (2014). Study of the combination reaction between drugs and bovine serum albumin with methyl green as a fluorescence probe. *J. Chem. Pharm. Res.* 6(5):968-974
- Hassan BAR (2012). Vitamins (Importance and Toxicity). *Pharmaceut. Anal. Acta* 3(8).
- Hegyi J, Schwartz RA, Hegyi V (2004). Pellagra: dermatitis, dementia, and diarrhea. *Int. J. Dermatol.* 43:1-5.
- Hemaiswarya S, Doble M (2010). Synergistic interaction of phenylpropanoids with antibiotics against bacteria. *J. Med. Microbiol.* 59:1469-1476.
- Jackson TM, Rawling JM, Roebuck BD, Kirkland JB (1995). Large supplements of nicotinic acid and nicotinamide increase tissue NAD<sup>+</sup> and poly(ADP-ribose) levels but do not affect diethylnitrosamine-induced altered hepatic foci in Fischer-344 rats. *J. Nutr.* 125:1455-1461.
- Khopkar SM (1998). Basic concepts of analytical chemistry. 2<sup>nd</sup> ed., New Delhi.
- Liptay W (1969). Electrochromism and solvatochromism. *Angew. Chem. Int. Ed. Engl.* 8:177-187.
- Liu RH (2003). Health benefits of fruit and vegetables are from additive and synergistic combinations of phytochemicals. *Am. J. Clin. Nutr.* 78: 517-520.
- Michale JL (1999). Molecular spectroscopy. USA: Prentice-Hall Inc.
- Mac Rae GE (1957). Theory of solvent effects on molecular electronic spectra. *J. Phy. Chem.* 61:562.
- Maiese K, Chong ZZ, Hou J, Shang YC (2009). The Vitamin Nicotinamide: Translating Nutrition into Clinical Care. *Molecules* 14:3446-3485.
- Milonni PW, Eberly JH (1988). Lasers. Wiley, New York.
- Nazzaro F, Caliendo G, Arnesi G, Veronesi A, Sarzi P, Fratianni F (2009). Comparative content of some bioactive compounds in two varieties of *capsicum annum* L. sweet pepper and evaluation of their antimicrobial and mutagenic activities. *J. Food. Biochem.* 33:852–68.
- Niazi A, Yazdanipour A, Ghasemi J, Kubista M (2006). Spectrophotometric and thermodynamic study on the dimerization equilibrium of ionic dyes in water by chemometrics method. *Spectrochim. Acta Part A* 65:73–78.
- Richelle M, Tavazzi I, Offord E (2001). Comparison of the antioxidants activity of commonly consumed polyphenols beverages (coffee, coca, and tea) prepared per cuping serving. *J. Agri. Food. Chem.* 49: 3438-3442.
- Rolfe HM (2014). A review of nicotinamide: treatment of skin diseases and potential side effects. *J. Cosmet. Dermatol.* 13:324-328.
- Schwab D (2001). Hepatic uptake of synthetic chlorogenic acid derivatives by the organic anion transport proteins. *J. Pharmacol. Exp. Ther.* 296:91-98.
- Shalita AR, smith JG (1995). Topical nicotinamide compared with clindamycin gel in the treatment of inflammatory acne vulgaris. *Int. J. Dermatol.* 34(6):434-437.
- Svilaas A, Sakhi AK, Andersen LF, Svilaas T, Strom EC, Jacobs JDR, Ose L, Blomhoff R (2004). Intake of antioxidants in coffee; wine and vegetables are correlated with plasma carotenoids in human. *J. Am. Nutr. Sci.* 134:562-567.
- Wang Z, Clifford MN, Sharp P (2008). Analysis of chlorogenic acids in beverages prepared from Chinese health foods and investigation, in vitro, of effects on glucose absorption in cultured Caco-2 cells. *Food Chem.* 108:369-373.
- Wen X, Takenaka M, Murota M, Homma S (2004). Antioxidative activity of a zinc chelating substances in coffee. *Bio. Sci. Biotechnol. Biochem.* 68(11):2313-2318.
- Williams A, Ramsden D (2005). Nicotinamide: a double edged sword. *Parkinsonism Relat. Disord.* 11:413-420.

*Full Length Research Paper*

# Baryte mineral exploration in parts of the lower Benue Trough, Nigeria

C. N. Ehirim\*, J. O. Ebeniro and C. O. Ofoegbu

Geophysics Research Group, Department of Physics, University of Port Harcourt, P. O. Box 122, Choba, Port Harcourt, Nigeria.

Received 19 August, 2016; Accepted 13 October, 2016

The use of DC electrical method in baryte mineral exploration has been investigated in Buruku northeast of Markurdi, Nigeria. The objective of the study was to investigate the suitability and potential of electrical resistivity tomography (ERT) combined with vertical electrical sounding (VES) surveys in baryte mineral exploration over known deposits. Results show that the interpreted layer resistivities correlate with the 2-D observations. The study delineated averagely 28 m deep symmetrically mound-shaped resistive anomalies (1500 to 5500  $\Omega$ m) encased within low resistive sandstone formation along prospective traverses. These responses are characteristics of probable vein structures associated with baryte mineralization. Two dominant E-W and NW-SE resistivity anomaly trends were delineated. The E-W trends were more prominent and persistent than the NW-SE. They are 25 to 50 m wide and stretches to over 300 m in length. The association of mineralized veins with these trends suggests that the veins must be of early Cretaceous age. These mineralized veins correlate with locations of known baryte deposits in the prospect area which hitherto, have been exploited by artisan miners. This is an obvious indication of the utility and resolution of dc electrical method in baryte mineral exploration in the area.

**Key words:** Electrical resistivity tomography (ERT), Vertical electrical sounding (VES), resistivity, Baryte, vein and mineralization.

## INTRODUCTION

Exploration and exploitation of solid minerals in Nigeria has remained comatose in the past decade, especially with the discovery of hydrocarbons in the Niger delta region. As the fortunes from hydrocarbons continue to dwindle with the growing instability in global demand and supply, attentions are now being focused on solid minerals as alternative sources of revenue and employment for the teeming population.

Most solid mineral occurrences in Nigeria are located in the Benue trough (Tate, 1959; Offodile, 1976). The trough is the failed arm of the triple junction formed as the African plate separated from the South American plate in the Pre-Cretaceous. It is a 1000 km NE-SW trending intra-continental Cretaceous basin resting unconformably on the basement complex. This is partitioned into the lower, middle and upper troughs with deposits of lead-

\*Corresponding author. Email: emekabridgy@yahoo.com.



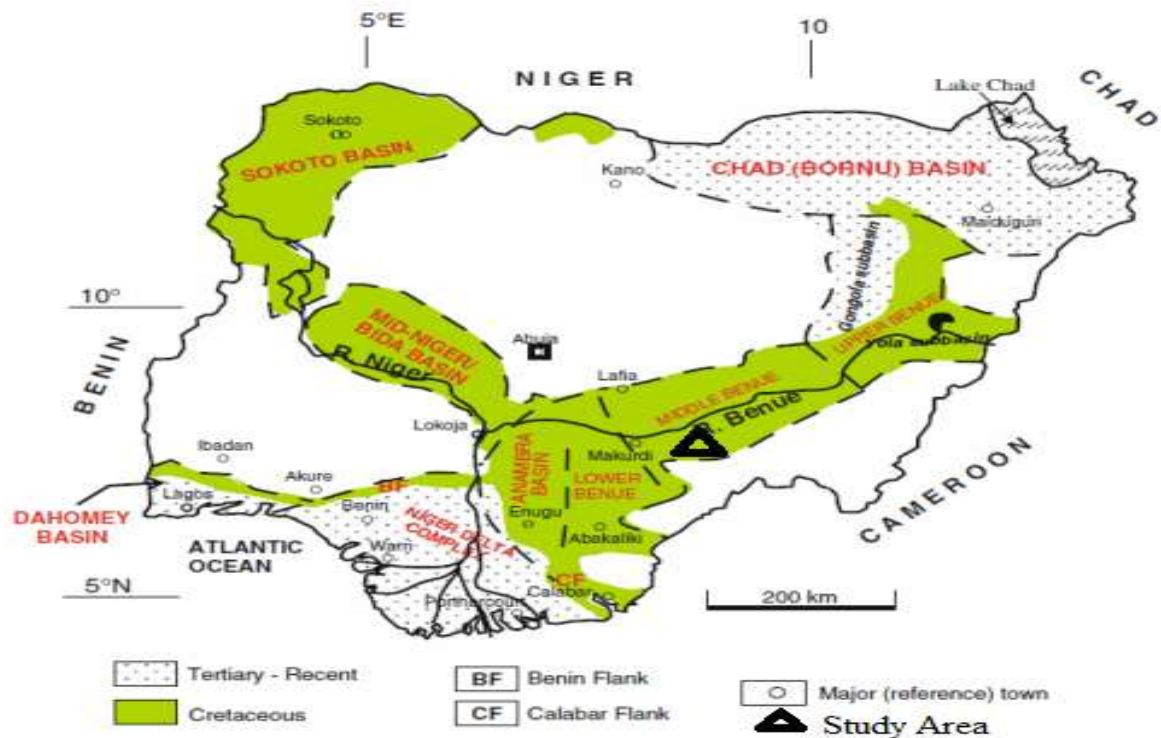


**Figure 1.** Location and geologic map of the study area (Adapted from Anthony et al., 2013).

zinc-baryte mineralization concentrated mostly in the lower and middle troughs (Farrington, 1952; Offodile, 1976).

The study area is located in Buruku NE of Markurdi, within the lower Benue depositional sub-basin and covers a total land area of (3060 x 900) m<sup>2</sup>. The topography in the study area is flat and gently undulating with little relief features which are somewhat dissected by valleys. The vegetation is typical of the Guinea savannah grass land with stunted shrubs and herbs in places (Figure 1).

The occurrence of baryte in parts of the trough has been reported by Farrington (1952), Tate (1959) and Offodile (1976), as epigenetic deposits arising from products of hydrothermal activity at shallow depths and low temperature. They occur as massive vein bound deposits and often times as a gangue mineral associated with lead-zinc mineralization in fractures, fissures, and open space fillings in sedimentary and igneous rocks. These veins are extremely varied in character and form. There are well developed in hard sandstone units and less likely in shales. The barytes in the trough are mostly the creamy white variety with a specific gravity of approximately 4.3, which is unusually heavy for a non-metallic mineral (Figure 2).

As the exploration for near-surface mineral deposits becomes more difficult due to complexities in geology, geophysical techniques are increasingly relied upon to identify areas of ore mineralization. Various geophysical

techniques have been adopted in the search for geobodies associated with mineralization (Bishop and Emerson, 1992; Maxwell, 2002; Mansour et al., 2008). These methods have developed rapidly over the last decade and each depends upon detecting variations in one or more of the physical properties of rocks (Electrical resistivity, Density, Magnetic susceptibility and Seismic velocities), which varies within wide limits.

Geophysical methods will be effective only if a target anomaly has a physical property contrast with the surrounding rock material. Baryte has a high resistivity compared to its host rock. This makes it easily detectable by the electrical method because of the resistivity contrast with the host rock. This forms the basis for the adoption of the electrical method in this study.

Electrical resistivity methods have variously been used in the exploration of baryte veins by several researchers (Egeh et al., 2004; Karen, 2004; Bhattacharya et al., 2006; Oladapo and Oladapo, 2011; Luano et al., 2012; Akpan et al., 2014; Obi et al., 2014). Results of study show that high resistivity signatures were diagnostic of baryte vein structures to which baryte mineralization could be associated. The resistivity of barytes depends on the BaSO<sub>4</sub> content, impurities and the environment of deposition.

The present study is aimed at evaluating the utility and resolution of dc electrical method in characterizing near surface mineralized baryte targets over known deposits and subsequently, delineate concealed baryte veins in



**Figure 2.** Exposed baryte veinlet in the study area.

the area. 2-D electrical resistivity tomography (ERT) and vertical electrical resistivity sounding (VES) surveys were employed for the study.

### Geology of the area

The study area is underlain almost exclusively by the Cretaceous Turanian Eze-Aku Formation. The formation consists of hard grey and black calcareous shale, limestone and siltstone (Figure 1). Locally, the shales grade into sandstone - Markurdi sandstones around Markurdi and environs. The formation is characterized by ferruginized sandstones and to a lesser extent quartz rocks and calcite (Offodile, 1976).

Baryte occur in lodes and veins infilling open fractures within sediments associated with Pb-Zn mineralization in the trough. Baryte mineralization in the prospect area occurred as a hydrothermal event, directly connected with the Mesozoic Magmatism during the early Cretaceous. Possible sources are the leaching of barium out of country rock by hydrothermal brines. Convection cells of meteoritic water, with upward-moving hydrothermal fluid being concentrated along the line occupied by fractures, offer a possible mechanism (Farrington, 1952; Offodile, 1976).

Many mineralized veins occupy E-W, NW-SE, and N-S fractures within the prospect area. The E-W trends give the strongest and most persistent veins and the N-S trend the weakest. Mineralization is structurally controlled and more or less confined to the limit of these faults (Chaanda et al., 2010; Wright, 1976).

### METHODOLOGY

#### Field methods

The study area measuring (3060 x 900) m<sup>2</sup> was divided into twenty (20) traverses of length 900m with inter traverse spacing's of approximately 150 m (Figure 3). 2-D electrical resistivity survey was

carried using constant separation profiling (or horizontal profiling) with Wenner alpha electrode configuration along each traverse perpendicular to the geologic strike (N-S). A digital read out Abem Terrametre SAS (signal averaging system) 1000C was used for the measurement of ground resistivity values. Measurements were made at sequences of increasing offset distance (a-spacing) along traverses ranging from 25, 50, 75, and 100 m, using twenty (20) electrodes. The electrodes were moved from one end of the line to the other in a lip frog manner till the traverse is completed. This was done for each of the traverses in the prospect.

Subsequently, vertical electrical soundings (VES) were carried out in selected traverses as confirmatory surveys based on the results of the 2-D resistivity survey. The Schlumberger electrode configuration with maximum AB/2 = 400m and MN/2 = 35 m were adopted, and a total of twenty (20) VES shot locations were occupied. The current electrodes were expanded about the mid-point of the suspected baryte vein on the surface and the potential electrodes (if necessary), to measure the vertical variation in resistivity. Data were processed and analyzed using resistivity softwares RES2DINV (2006) and IPI2WIN (2003) for ERT and VES respectively, for subsequent interpretation.

### RESULTS PRESENTATION

The results of study are presented as 2-D electrical inverse model sections (Tomogram) and 1-D vertical electrical sounding model curves. These resistivity models generally exhibit root mean square (RMS) errors varying from 0.1 to 5.7%, a reflection of the degree of fit between the calculated and field data. This guarantees the use of the models for subsequent analysis and interpretation. The models were visually inspected and zones/layers of anomalously high resistivity values were isolated from the lows and characterized in space in the study area.

The 2-D resistivity models are characterized by extensive symmetrically mound-shaped high resistivity anomalous features encased in low resistive materials as host rock. Their resistivities vary from 1,500 to over 5,500  $\Omega$ m. A typical model inverse section along traverse 12 is shown in Figure 4. Two symmetrically mound-shaped high resistivity anomalies (>4,811  $\Omega$ m) were delineated to

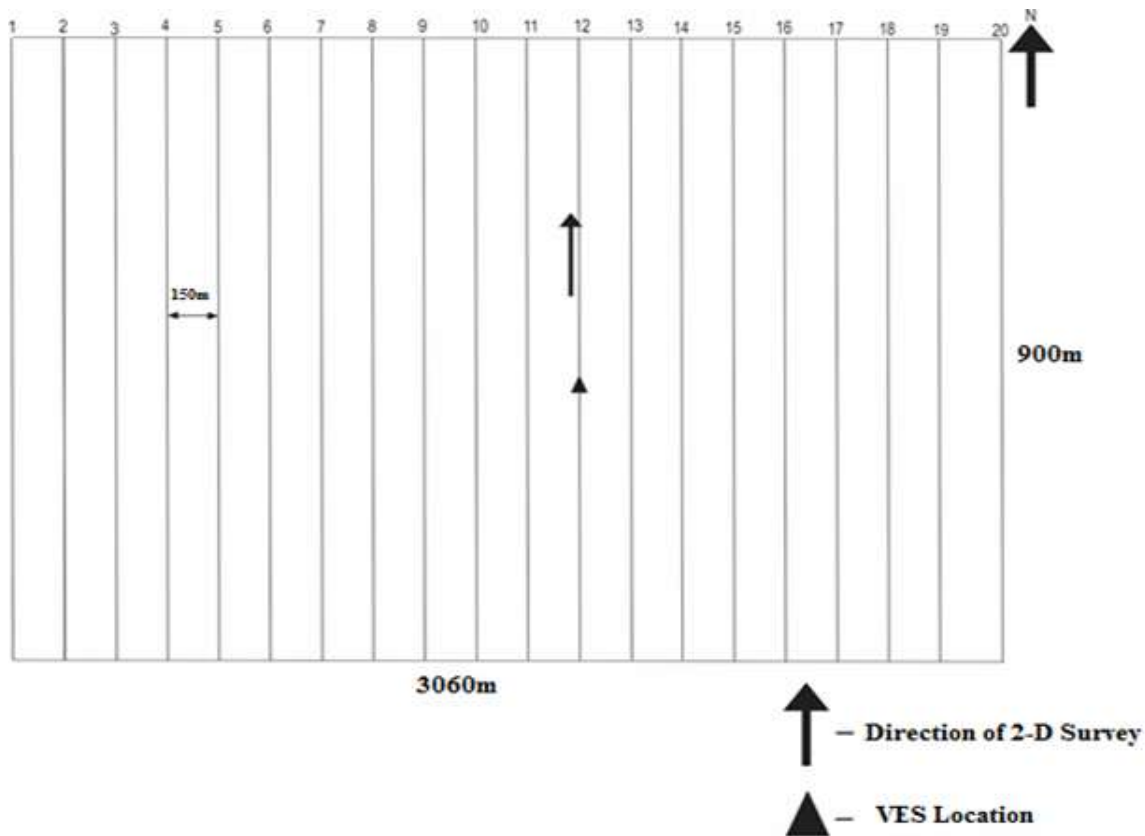


Figure 3. Traverse or grid lines for the electrical survey in the study.

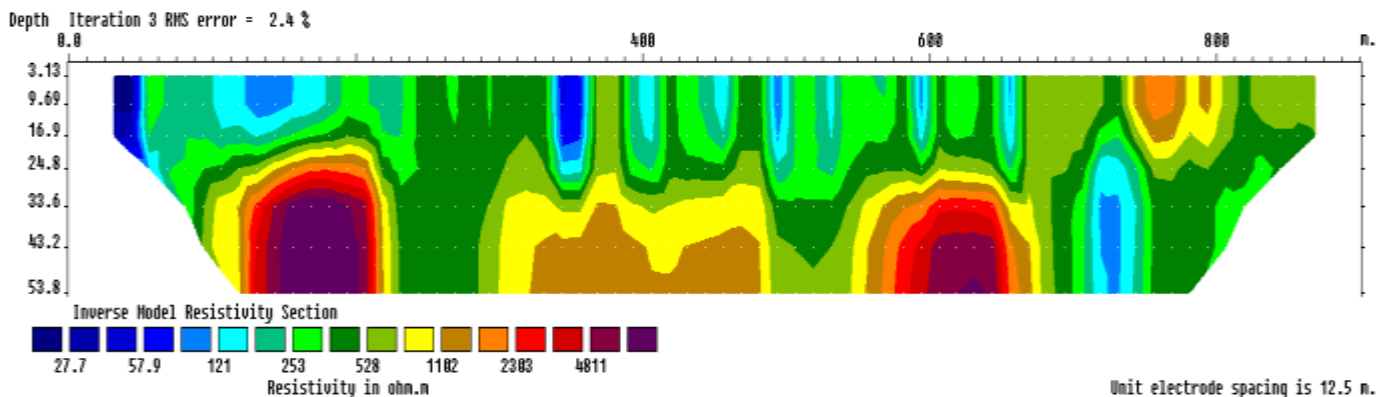


Figure 4. Typical 2-D profile along traverse 12 in the study area.

the north and south of the traverse flanked by low resistive host rock.

These are situated at 175 and 625 m surface points with tops at 24 and 28 m subsurface depths, respectively, with an average thickness of 43 m. The base of the structure extends beyond 53 m subsurface depth, which probably suggests mineralization at deeper depth. These resistive structures exhibits gradational variations in colour scale related to probably distinct zonation in

mineral content with depth. The zonation is outward and upward from the base of the structures. This response is characteristic of a vein type structure accompanied by high resistivity to which baryte mineralized veins can be inferred.

Vertical electrical sounding (VES) survey conducted at 175 m surface point to the midpoint of the first resistive structure along traverse 12, revealed a 7-layer geoelectric section (Figure 5). The lithology varies from

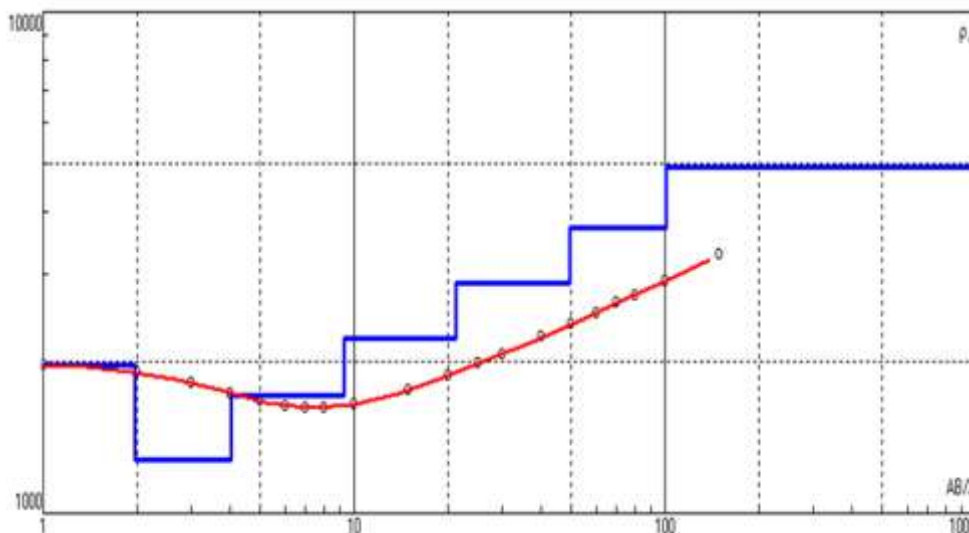


**Figure 5.** Typical VES curve along Transverse 12 in the study area.

**Table 1.** A typical interpreted VES model along Transverse 12.

Layer No.	Rho ( $\Omega\text{m}$ )	Depth (m)
1.	1984	1.98
2.	1280.0	4.02
3.	1723.0	9.25
4.	2237.0	21.34
5.	2885.0	49.35
6.	3720.0	101.40
7.	4970.0	

top soil of sands/quartz and lateritic materials to sandstone successions with anomalously high resistivity signatures at increasing depth (Table 1). Baryte target were delineated at the depth of 21.34 m with high resistivities varying from 2237 to > 4970  $\Omega\text{m}$  and at depth extending beyond 100 m.

These results are comparable to the 2-D electrical resistivity observations. It therefore means that these symmetrically mound-shaped high resistivity anomalies are unlikely to be simply altered and deformed sedimentary rocks. There are therefore, interpreted as probable baryte mineralized veins in the prospect area.

Based on these observations, resistivity and depth contour maps of the isolated baryte veins were generated to characterize their quality and depth distribution in space in the prospect area. The depth contour map (Figure 6) revealed that the depths to the top of these structures are shallow in the western and mid-western parts (Bright shades) with depth range of 25 to 30 m, than the south, central and eastern parts (Dark shades) associated with depths exceeding 30 m.

The 3-D depth structure profile show a structural anomaly high along the E-W trend flanked by structural lows to the central and southern parts of the prospect (Figure 7). The highs correspond to shallow mineralized veins, while the lows to the deeply buried veins. The mineralized veins trends dominantly in the E-W and NW-SE and less in the NE-SW of the prospect. The VES shot points at the midpoint of the structures are indicated by vertical solid lines capped with the VES numbers (in red).

The resistivity contour map (Figure 8) show that the deeply buried veins to the southern, central and eastern parts of the prospect exhibits high resistivities than the western and mid-western shallow targets. This suggests that pure and high quality baryte mineralized veins exist in the southern, central and eastern parts at greater depths (>30 m) and poor quality baryte veins in the shallow western and mid-western parts (<30 m). The solid vertical lines are the centers of the veins along traverses capped with the depth to the top of the structures (in red).

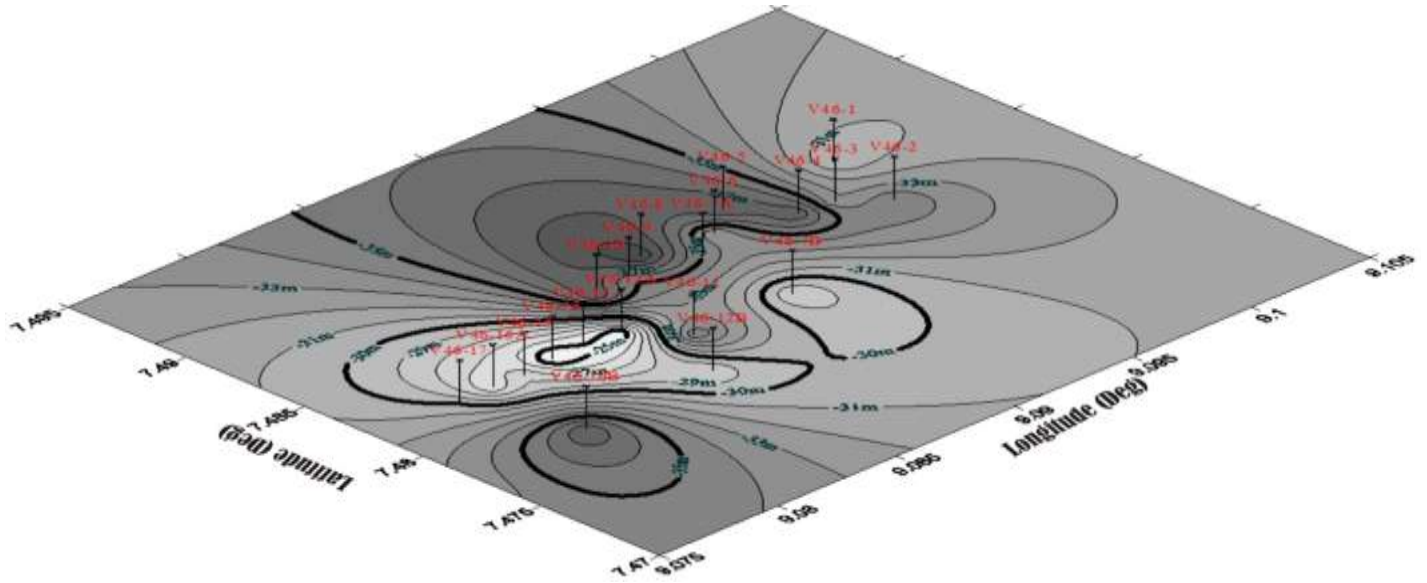


Figure 6. Depth contour map of the prospect area.

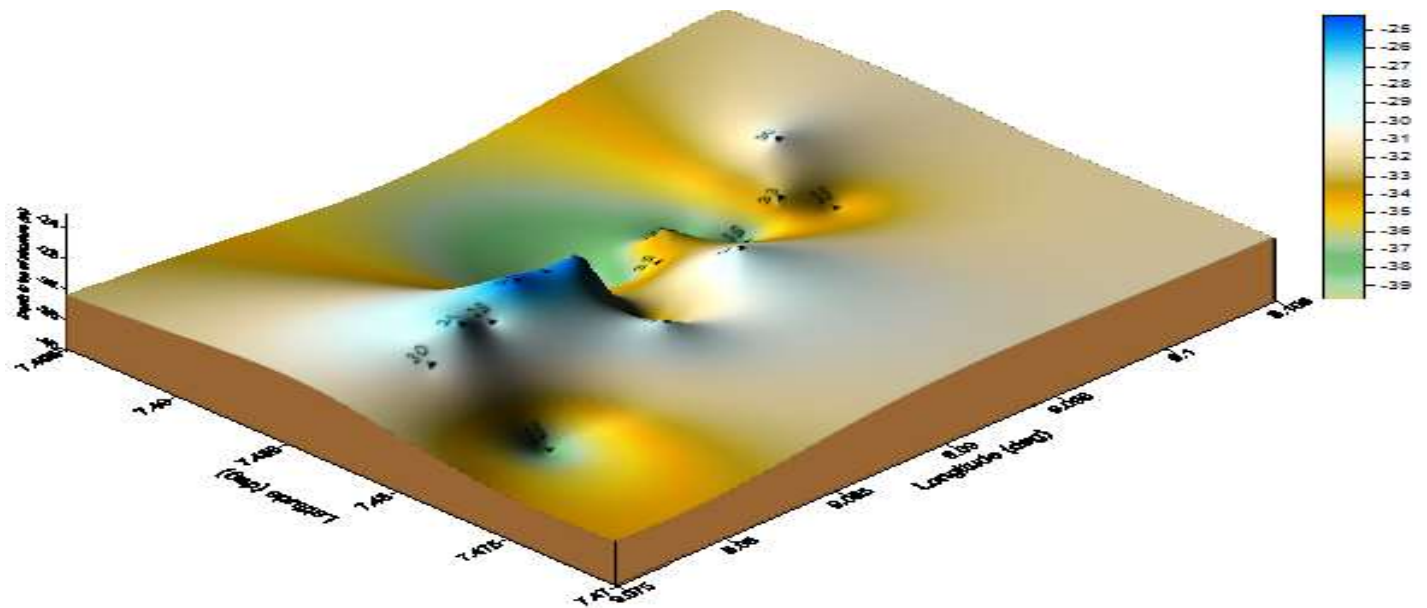


Figure 7. 3-D depth structure profile of the prospect area.

## DISCUSSION

2-D electrical resistivity tomography (ERT) and Vertical electrical resistivity (VES) direct current electrical methods were adopted in the exploration of baryte mineralized veins in the study area. Results show that the prospect area is characterized by complex geological structures with anomalously varying resistivities along traverses, related to regional and local anomalous values. The regional anomalies are related to the surface

and subsurface variations in lithologic units and their contacts, while the local anomalies correspond to possible mineralized veins along the investigated traverses.

2-D electrical resistivity tomography (ERT) model sections exhibit symmetrically mound-shaped high resistivity structures encased by low resistive sandstones. This encasing sandstone seems the most promising host rock for vein mineralization in the study area. The geometrical and essentially symmetric nature of the

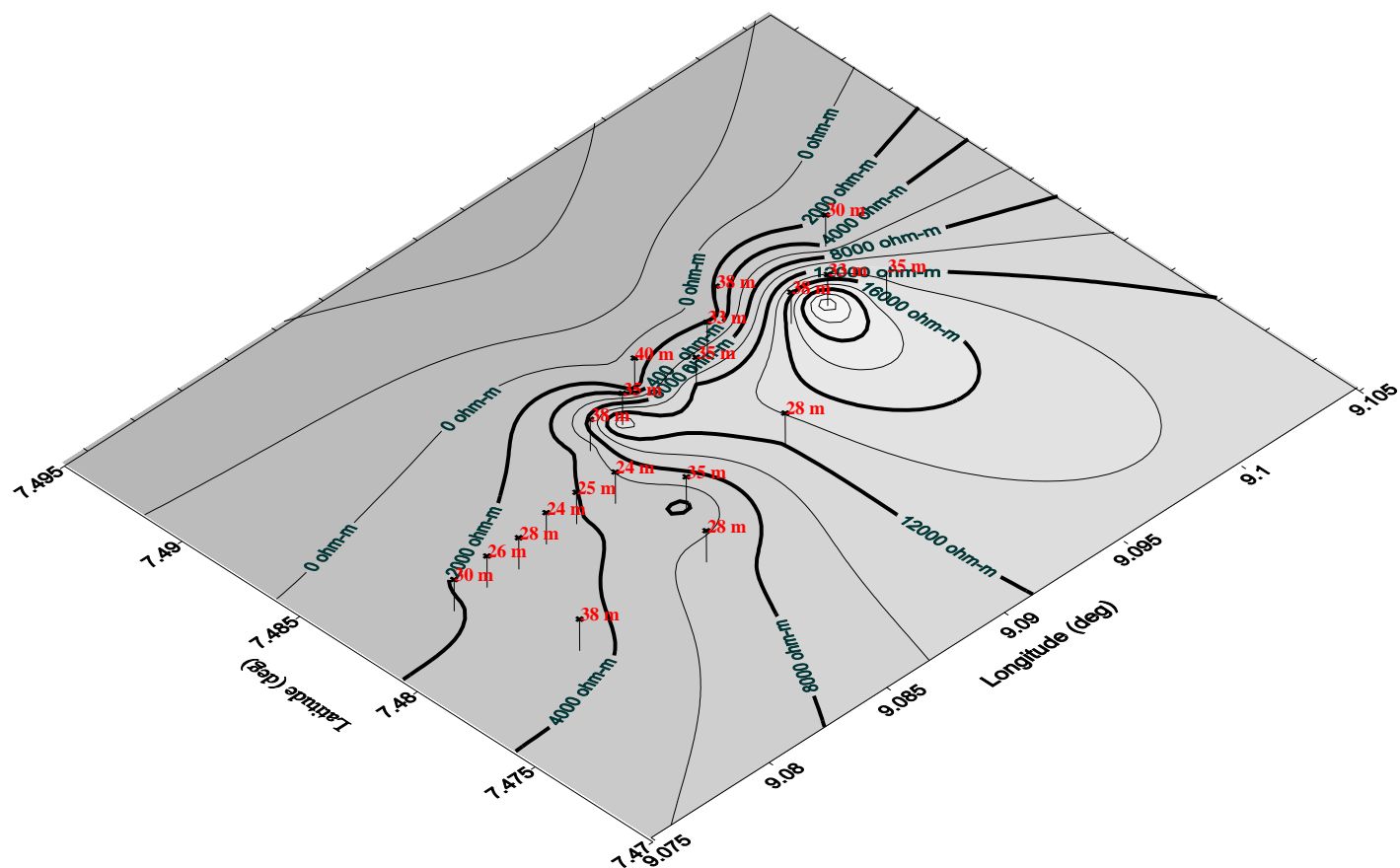


**Figure 8.** Resistivity contour map of the prospect area.

electric anomalies suggests that the source is a massive and narrow vertical body buried at depth. Vertical electrical sounding (VES) shot at the midpoint of these suspected mineralized baryte targets along prospective traverses exhibits increasing anomalously high resistivity signatures with increasing layer depths, which correlates with baryte mineralization.

The study revealed the presence of averagely 28 m deep suspected baryte mineralized veins in the prospect area, with high resistivities of 1500 to 5500  $\Omega\text{m}$ . Formation resistivities greater than this, are interpreted as intruding plugs of fresh basement rocks in the sedimentary sequence. The width of the mineralized veins varies from 25 to over 50 m, and extends to over 300 m in length in prospective traverses. The veins are wider than normal probably because of the lithology and competence difference which affects the inclination of fault planes and vein development in the sediments.

Baryte targets are shallow in the west and mid-western parts (< 25 m) than the southern, central and eastern parts (> 30 m) of the prospect. The deeply buried veins to the southern, central and eastern parts of the prospect exhibits higher resistivities than the west and south western shallow veins and as such, are probably of

higher quality and economic value. This could be attributed to dipping associated with the prevailing structural trends concomitant with increasing mineral content along the down thrown part of the veins.

Dominant E-W and NW-SE resistivity anomaly trends were delineated. The E-W trends were more prominent and persistent than the NW-SE trend. These electrical anomaly trends stretches to over 300 m in length and generally exhibit minor variations in path length, while maintaining their dominant trend axes. This suggests structural control of mineralization in the prospect area. The striking association of mineralized veins with the E-W and NW-SE fault trend suggests that the veins must be of early Cretaceous age (Tate, 1959; Farrington, 1952; Offodile, 1976). This implies that baryte may have been emplaced by space filling rather than by replacement along E-W steeply dipping to vertical veins cut by minor SE mineralized veins. This suggests a tensional regime culminating in mineralization along structural trends in the prospect area.

According to the works of Oladapo and Oladapo (2011), Luaano et al. (2012), Oden (2012), Akpan et al. (2014) and Obi et al. (2014), high resistivity/low conductivity anomalous values are diagnostic of baryte

mineralized veins to which barytes can be associated. The resistivity of baryte mineralized veins ranges from 1300-3999  $\Omega\text{m}$ , which may likely vary within a wide margin dependent on impurities and  $\text{BaSO}_4$  content. The high resistivity of the barytes is due to its very low intergranular porosities associated with its high density. The authors also reported baryte veins having thicknesses ranging from 17.1 to 60.7 m, with an average thickness of 38 m, predominantly NW-SW and NE-SW trends and subsurface baryte target depth of 37.4 m in the study areas. These observations compare fairly well and validates the results of the present study in the area.

These mineralized veins correlates with locations of abandoned and working mine pits exploited by artisan miners through surface mining. The artisan miners are merely exploiting exposed surface veins which do not persist over long distances and depth. However, the potential for massive and persistent mineralized baryte veins is high at greater depths based on the results of this study.

## Conclusion

The combination of 2-D and VES dc electrical methods proved to be effective and robust in delineating baryte mineralized veins in the study area. The study revealed the presence of averagely 28m deep and 1500 to 5500  $\Omega\text{m}$  resistive electrical anomalies related to baryte mineralized veins along E-W and NW-SE resistivity anomaly trends.

The association of baryte mineralized veins with these fracture systems is indicative of the fact that the veins must be of early Cretaceous age. This suggests that baryte mineralization in the prospect area probably, postdates these fracture systems at shallow depths. This implies that baryte may have been emplaced by space filling rather than by replacement along E-W steeply dipping to vertical veins cut by minor SE mineralized veins, suggesting a tensional regime culminating in mineralization along structural trends.

These mineralized veins correlates with locations of abandoned and working mine pits exploited by artisan miners through surface mining. This indicates the utility and resolution of dc electrical method in baryte mineral exploration.

## Conflict of Interests

The authors have not declared any conflict of interests.


## ACKNOWLEDGEMENT

The authors express appreciation to the Mining Division of Resources Management and Manufacturing Co.

Limited for their technical support and permission to use data for this study, without which we would not have succeeded.

## REFERENCES

- Akpan AE, Ebong D, Ekwok SE, Joseph S (2014). Geophysical and Geological studies of the spread and industrial quality of Okurike barite deposit. *Am. J. Environ. Sci.* 10(6):566-574.
- Anthony TB, Sunday OI, Alege TS (2013). Economic Aspects of Carbonates of the AlbianAsu River Group in Tse-Kuchanearyandev, Middle Benue Trough, Nigeria. *J. Geogr. Geol.* 5(2):13-21.
- Bhattacharya BB, Shiktar CJ, Mallick K (2006). Geophysical prospecting for baryte. *Geophys. prospecting* 22(3):421-429.
- Bishop JR, Emerson DW (1992). Geophysical properties of zinc bearing minerals. *Austr. J. Earth Sci.* 46:311-328.
- Chaanda MS, Obaje NG, Moumouni A, Goki NG, Law UA (2010). Environmental Impact of Artisanal Mining of Barytes in Azara Area, Middle Benue Trough Nigeria. *J. Earth Sci.* 4(1):38-42.
- Egeh EU, Ekwuemeke BN, Akpeke BG (2004). The appraisal of a proposed barite quarry in Akpet Area, Cross River State from resistivity investigation. *Glob. J. Geol. Sci.* 2(2):171-175.
- Farrington JL (1952). A preliminary description of the Nigerian lead-zinc field." *Bull. Soc. Econ. Geol.* 47(6):18-32.
- IPI2Win (2003). "Resistivity sounding interpretation software, version 3.0." Moscow State University, 2003.
- Karen K (2004). A special issue devoted to baryte and Zn-Pb -Ag deposits in the red dog district, western Brooks Range, Northern Alaska. *Econ. Geol.* 99(7):1267-1280
- Luaano L, Horacio E, Mario T, Marta A, Ricardo E (2012). Geoelectric exploration of the Purisima-Kumicruze district, Jukay Province, Argentina. *Int. J. Geophys.* 2012:1-12.
- Mansour AA, Hesham MH, Abdelmonem AE, Hamdy IH, Hesham ME (2008). Reconnaissance Geophysical and Geological Studies on Bahrah prospect, Makkah Al-Mukarramah Region KSA. *Earth Sci.* 19:159-190.
- Maxwell AM (2002). Geoelectromagnetic Exploration for Natural Resources: Models, Case studies and Challenges. *Surv. Geophys.* 23:133-205.
- Obi AA, Ekwueme BN, Akpeke GB (2014). Reserve estimation of baryte deposits using geological and geophysical investigation in Cross Rivers South eastern Nigeria. *J. Environ. Earth Sci.* 4(10):16-31.
- Oden MI (2012). Barite veins in the Benue trough: Field characteristics, the quality issue and some tectonic implications. *Environ. Nat. Resour. Res.* 2(2):1-11.
- Offodile ME (1976). Review of the geology of the Cretaceous Benue Valley, in *Geology of Nigeria* (C. A. Kogbe Ed.) Elizabethan Publishing Coy, Lagos.
- Oladapo MI, Oladapo OOA (2011). Geophysical investigation of barite deposits in Tunga, North eastern Nigeria. *Int. J. Phys. Sci.* 6(20):4760-4774.
- RES2DINV (2006). Geoelectrical imaging of 2D data, Geotomo software, Penang, Malaysia.
- Tate RB (1959). Geological Survey of Nigeria (GSN) Report No.1266.
- Wright AE (1976). Review of the Origin and Evolution of the Benue Trough in Nigeria. *Depth of Earth Sciences*, Open University Milton-Kegnes, Great Britain.



# International Journal of Physical Sciences

Related Journals Published by Academic Journals

- *African Journal of Pure and Applied Chemistry*
- *Journal of Internet and Information Systems*
- *Journal of Geology and Mining Research*
- *Journal of Oceanography and Marine Science*
- *Journal of Environmental Chemistry and Ecotoxicology*
- *Journal of Petroleum Technology and Alternative Fuels*



**academicJournals**